A multifunctional mechanical metamaterial with adjustable density, stiffness, Poisson's ratio, and thermal expansion
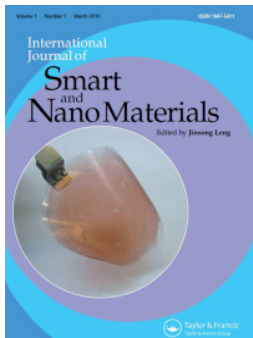
Tian, Jiayu; Guo, Yaqi; Shi, Chuanqian; Zhao, Ying

Important note
To cite this publication, please use the final published version (if applicable).
Please check the document version above.

A multifunctional mechanical metamaterial with adjustable density, stiffness, Poisson's ratio, and thermal expansion

Jiayu Tian, Yaqi Guo, Chuanqian Shi & Ying Zhao

View supplementary material

Published online: 17 Aug 2025.

Submit your article to this journal

Article views: 152

View related articles

View Crossmark data

Taylor & Francis
Taylor & Francis Group

A multifunctional mechanical metamaterial with adjustable density, stiffness, Poisson's ratio, and thermal expansion

Jiayu Tian[a], Yaqi Guo[b], Chuanqian Shi[c] and Ying Zhao[a]

[a]School of Aerospace Engineering and Applied Mechanics, Tongji University, Shanghai, China; [b]Department of Materials Science and Engineering, Delft University of Technology, Delft, The Netherlands; [c]Center for Mechanics Plus under Extreme Environments, School of Mechanical Engineering & Mechanics, Ningbo University, Ningbo, China

ABSTRACT

Mechanical metamaterials have garnered significant attention in materials and mechanics due to their unique geometric designs and tunable properties. However, metamaterials that allow for simultaneous multi-parameter control remain relatively scarce. This study introduces a multifunctional mechanical metamaterial where density, Young's modulus, Poisson's ratio, and thermal expansion coefficient are coordinately tunable through a combination of geometric design and material distribution. The influence of geometric and material parameters on the effective properties of the proposed metamaterial was systematically investigated through analytical solution, finite element simulation and experimental measurement. The results demonstrate that adjusting geometric parameters enables the structure to achieve a combination of lightweight characteristics, high adaptability, and negative Poisson's ratio. Furthermore, the introduction of heterogeneous materials, leveraging the thermal strain mismatch at their interfaces, allows for simultaneous control over the structure's thermal deformation, enabling either negative or positive thermal expansion. These combined properties are difficult to achieve with existing natural or artificial materials. This work can provide potential applications in flexible devices, smart structures, and thermal management.
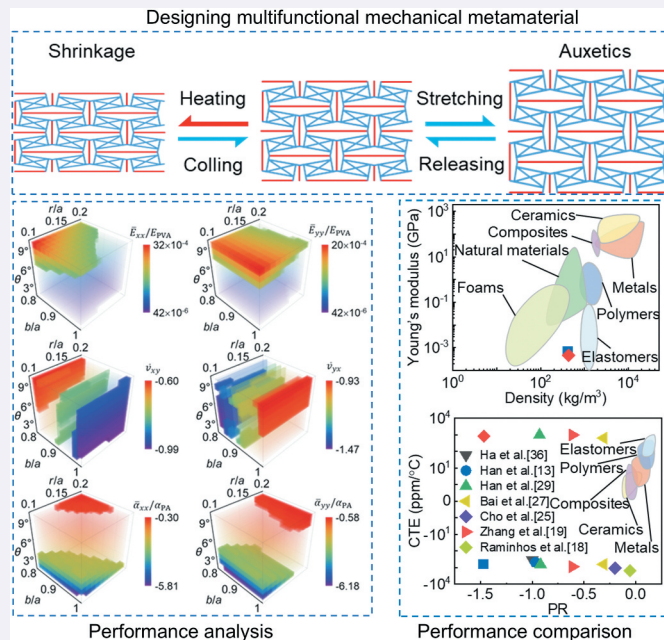
Designing multifunctional mechanical metamaterial

1. Introduction

Mechanical metamaterials have garnered significant attention in the field of materials and mechanics because of their unique geometric design and tunable properties [1–4]. These metamaterials can exhibit some extraordinary mechanical properties, such as negative Poisson's ratio [5–8] (PR) and thermal expansion coefficient [9–12] (CTE), which are difficult to achieve with conventional materials in nature. In recent years, researchers have been making continuous efforts to further expand the functions of mechanical metamaterials, so that they can simultaneously regulate multiple parameters to meet the needs of more complex applications. For example, the bi-material composite lattices demonstrate that unconventional properties like negative PR and negative CTE can be simultaneously achieved through strategic geometric arrangements [13–18]. The concept of multifunctional mechanical metamaterials came into being, which aims to realize the coordinated control of several key mechanical parameters such as PR and CTE.

Based on different deformation modes, the multifunctional mechanical metamaterials can be primarily categorized into tension-dominated [15,19–24], bending-dominated [25–27], and hybrid types [13,28,29]. Each type possesses its own advantages and disadvantages. For instance, tension-dominated types typically exhibit higher stiffness but offer a narrower range of achievable PR and CTE values. While bending-dominated types can achieve a broader range of PR and CTE values, they generally possess relatively lower stiffness. In contrast, hybrid types can achieve an intermediate range of stiffness, PR, and CTE values, involving more trade-offs among these properties. Despite notable advancements in the field of multifunctional metamaterials, significant limitations exist in current designs. Many designs prioritize the enhancement of certain mechanical performance, such as stiffness [11,30–32], but fall short in adaptability and versatility for various applications. On the other hand, while structures exhibiting a combination of auxeticity and tunable thermal expansion have been reported, their accessible parameter ranges remain constrained. For instance, reported negative PR values are mostly unable to reach below −1 [13,29,33,34], and the majority of achievable CTE is limited to a range between 98 and −661 ppm/ºC, [13] due to inherent structural constraints. While notable exceptions exist, such as the work by Tian et al. [35], who demonstrated a functional mechanical metamaterial based on a rotating rectangular geometry and bi-material distribution, thereby expanding the accessible ranges for both negative PR and CTE, such studies often present incomplete analyses. They primarily focused on characterizing the PR and CTE of their proposed structure, but a comprehensive analysis of crucial properties such as density and Young's modulus (YM) is notably absent. Furthermore, a corresponding analytical model capable of predicting and explaining the observed behavior remains to be developed. These challenges underscore the need for more holistic design strategies and comprehensive analytical frameworks to fully realize the potential of multifunctional metamaterials.

In this work, we propose a bi-material multifunctional mechanical metamaterial that can achieve coordinated control over density, YM, PR, and CTE. To elucidate the underlying mechanisms governing the behavior of this metamaterial, we derived an analytical model that is verified with finite element simulations. This model was employed to systematically analyze the influence of key geometric parameters – the rotation angle, rotating-rectangle aspect ratio, and in-plane thickness of material and the material distributions – on the aforementioned properties, including density, YM, PR, and CTE. Based on these analyses, we demonstrate that judicious geometric design can achieve a structure that integrates lightweight characteristics (density < 0.44 g/cm^3), high adaptability (YM < 67 MPa), and auxetic behavior (Figure 1, PR up to −1.47). Furthermore, by incorporating heterogeneous materials, we exploit the interfacial thermal strain mismatch between these
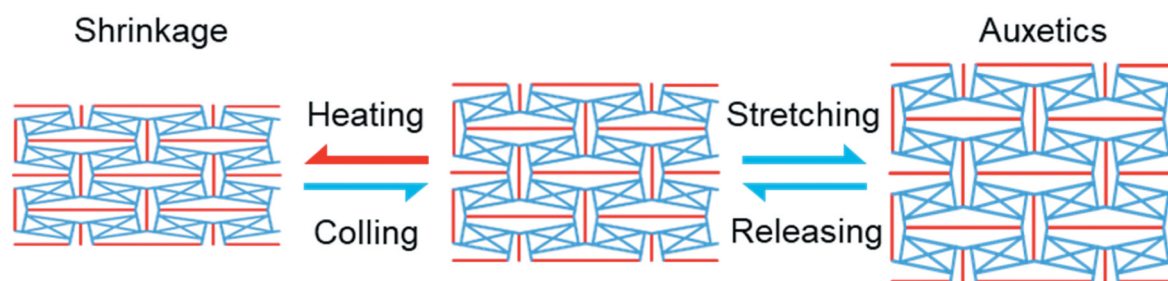

Figure 1. Multifunctional mechanical metamaterial with thermal shrinkage and auxetic behavior.

materials to achieve macroscopic thermal deformation control (CTE from −630 ppm/ºC to 850 ppm/ºC), allowing for tunable thermal contraction or expansion (Figure 1). This work provides an analytical framework of the performance of multifunctional mechanical metamaterial and further expansion of the adjustable performance parameters.

2. Models and methods

2.1. Geometry of the multifunctional mechanical metamaterial

As illustrated in Figure 2, the multifunctional mechanical metamaterial has a two-dimensional lattice configuration, composed of periodically arranged heterogeneous rectangular beams with two materials, denoted by material 1 (M1) and material 2 (M2). This structural system is constructed by expanding a representative volume element (RVE) shown in Figure 2 through two-dimensional array replication in the x-y plane. The RVE contains four rotating rectangles with mirror symmetry and connecting beams, with its geometrical characteristics determined by six key parameters: length a and width b of the rotating-rectangle, rotation angle θ, in-plane thickness of M1 (t_1) and M2 (t_2), and lateral extension length r. The out-of-plane thickness of all components is uniformly set to a fixed value h. To ensure structural feasibility, the following geometric constraints must be met: 1) $t_1 + t_2 \leq 2R$, 2) $b \leq a$, 3) $0 < \theta < 45°$.

2.2. Analysis of effective thermoelastic constants

Since the structure does not require significant strain for each beam, it is assumed that both materials (M1 and M2) behave thermoelastically linear. The associated material parameters (M1 and M2) are E_1 and E_2 for YM, v_1 and v_2 for PR, and α_1 and α_2 for CTE. From a macroscopic perspective, the structure can be treated as a homogeneous continuum medium with effective thermoelastic properties. Owing to its geometric symmetry, the system exhibits thermoelastic orthotropy. In the current configuration, the coordinate axes align precisely with the orthogonal principal axes of the unit cell (Figure 2), thereby eliminating shear-tension /compression coupling terms in the effective stiffness tensor and nullifying non-axial components of the thermal expansion tensor. Given the exclusive focus on planar thermoelastic behavior, the effective constitutive relationship derived through volume-averaged thermoelastic Hooke's law can be formulated as:

$$
\begin{bmatrix} \bar{\sigma}_{xx} \\ \bar{\sigma}_{yy} \\ \bar{\sigma}_{xy} \end{bmatrix} = \begin{bmatrix} \bar{C}_{11} & \bar{C}_{12} & 0 \\ \bar{C}_{12} & \bar{C}_{22} & 0 \\ 0 & 0 & \bar{C}_{66} \end{bmatrix} \begin{bmatrix} \bar{\varepsilon}_{xx} - \bar{\alpha}_{xx}\Delta T \\ \bar{\varepsilon}_{yy} - \bar{\alpha}_{yy}\Delta T \\ 2\bar{\varepsilon}_{xy} \end{bmatrix} \tag{1}
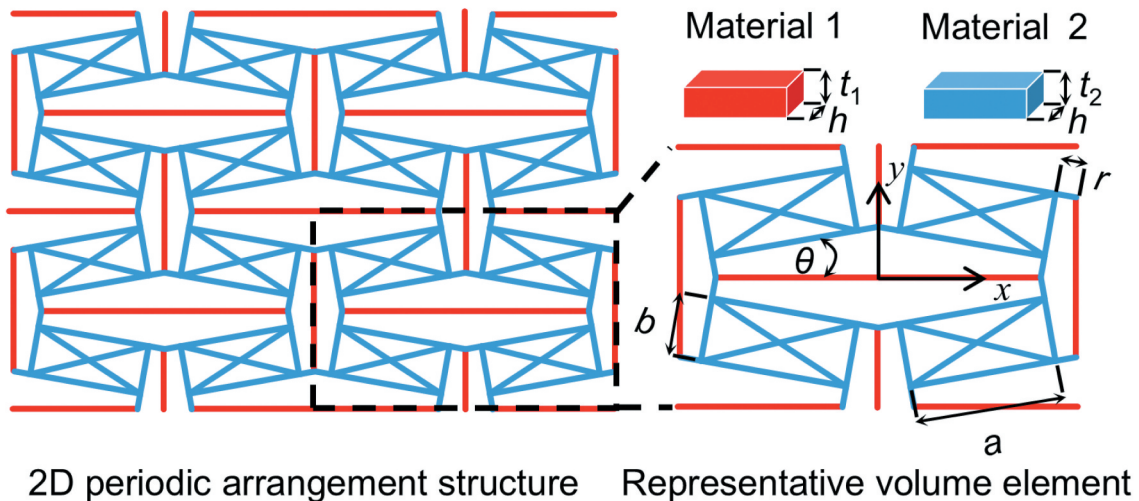$$

Figure 2. The multifunctional mechanical metamaterial and it's representative volume element.

where $\bar{a}_{xx}$ and $\bar{a}_{yy}$ represent the effective CTE. Based on Eq (3), we can conveniently evaluate the effective YM $\bar{E}_{xx}$ and $\bar{E}_{yy}$, and PR $\bar{v}_{xy}$ and $\bar{v}_{yx}$ through the following expressions:

$$\bar{E}_{xx} = \frac{\bar{C}_{11}\bar{C}_{22} - \bar{C}_{12}^2}{\bar{C}_{22}} \tag{2}$$

$$\bar{E}_{yy} = \frac{\bar{C}_{11}\bar{C}_{22} - \bar{C}_{12}^2}{\bar{C}_{22}} \tag{3}$$

$$\bar{v}_{xy} = \frac{\bar{C}_{12}}{\bar{C}_{22}} \tag{4}$$

$$\bar{v}_{yx} = \frac{\bar{C}_{12}}{\bar{C}_{11}} \tag{5}$$

Leveraging the structural periodicity and symmetry, the effective thermoelastic properties are determined through computational homogenization of a quarter-RVE domain under periodic boundary conditions. Each constituent beam is explicitly modeled as a Timoshenko beam with a rectangular cross-section. The closed-form expressions for the effective thermoelastic parameters – including orthotropic effective YM ($\bar{E}_{xx}$ and $\bar{E}_{yy}$), PR ($\bar{v}_{xy}$ and $\bar{v}_{yx}$), and CTE ($\bar{a}_{xx}$ and $\bar{a}_{xy}$) – are derived in detail in Appendix A of Supplementary Material.

2.3. Finite element analysis

A two-dimensional parametric numerical model was established based on finite element analysis (FEA) to numerically determine the effective thermoelastic constants of the multifunctional deformable structure. The geometric modeling strictly follows the configuration characteristics of RVE, including the distribution of materials and symmetric arrangement of rotating rectangles. Linear elastic constitutive models were employed. The beam components were discretized using Timoshenko beam elements. Through the mesh sensitivity analysis (Figure S1 of Supplementary Material), a global mesh size set to 0.001 mm to achieve optimal balance between computational efficiency and accuracy. For the boundary condition, periodic boundary conditions defined by Equation (8) were applied to the unit cell (Figure 3). The static implicit solver combined with Newton-Raphson iteration method was employed for solution.

$$\begin{cases} u_i^{upper} - u_i^{lower} = \bar{\varepsilon}_{ij}\left(x_j^{upper} - x_j^{lower}\right), (i,j = 1,2) \\ u_i^{right} - u_i^{left} = \bar{\varepsilon}_{ij}\left(x_j^{right} - x_j^{left}\right), (i,j = 1,2) \end{cases} \tag{6}$$
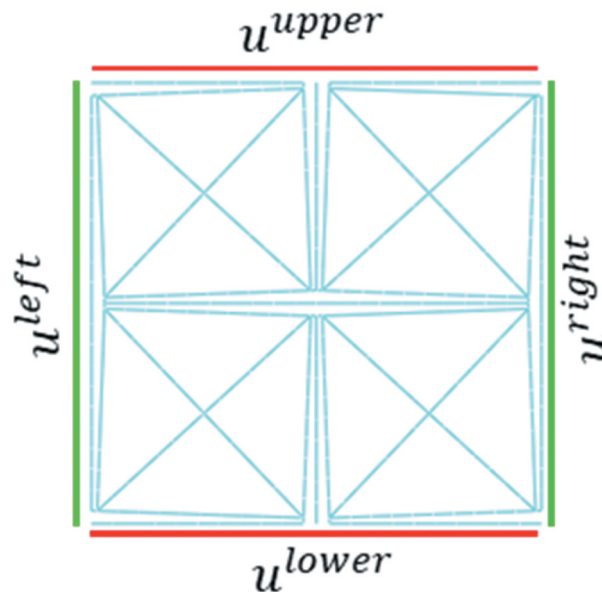

Figure 3. A representative volume element with periodic boundary conditions.

Here, u_i^{upper}, u_i^{lower}, u_i^{right} and u_i^{left} denote the displacement components along the i-direction at corresponding points on the upper, lower, left, and right boundaries, respectively. $\bar{\varepsilon}_{ij}$ represents the components of the macroscopic homogeneous strain tensor (satisfying $\bar{\varepsilon}_{ij} = \bar{\varepsilon}_{ji}$), while $x_j^{upper} - x_j^{lower}$ and $x_j^{right} - x_j^{left}$ correspond to the periodic spacing vectors in the vertical and horizontal directions, respectively.

2.4. Experiments

Due to the multifunctional mechanical metamaterial being composed of two different materials, and considering the feasibility of the process, a multi-material fused deposition modeling 3D printer was used for the integrated fabrication of the specimens. The polyvinyl alcohol (PA) and polyamide (PVA) were used as the component material of the multifunctional mechanical material. The dynamic mechanical analysis (MCR102e, Anton Paar) and electronic universal testing machine (ST100KN, Tinius Olsen) were used to measure key performance parameters such as the storage modulus, YM, PR, and CTE of PVA and PA materials. The storage modulus of both materials exhibits minimal variation within the temperature range of 20–50°C (Figure S2a of Supplementary Material). The thermal strain of both materials changes linearly within this temperature range (Figure S2b of Supplementary Material). Therefore, constant values for YM and CTE are used in the theoretical and simulation models. The static tensile stress-strain curves for both materials are presented in Figure S1c of Supplementary Material. Through determined, the relevant material properties were shown in Table 1.

The specimens and specific printing process are shown in Figure 4: the geometric configuration of the printed sample is consistent with the theoretical representative unit, and through a dual-nozzle cooperative

Table 1. Material properties of PA and PVA.

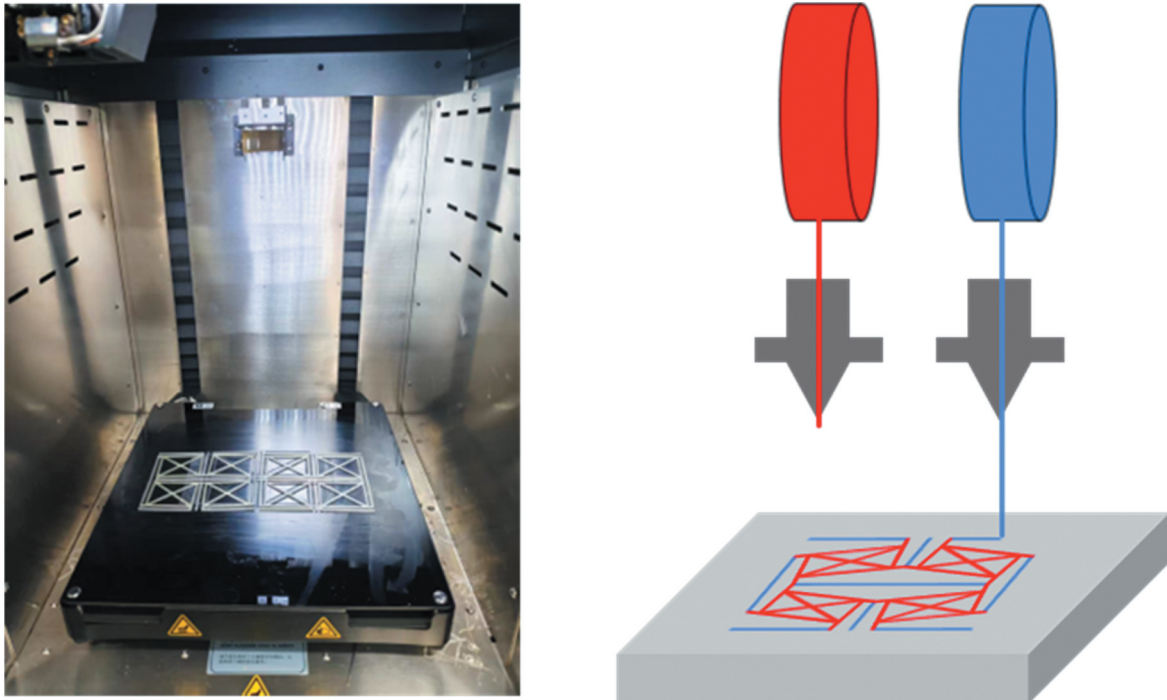| Parameter (Material)	PVA	PA
Density	1.37 g/cm^3	1.12 g/cm^3
YM	1460 MPa	928 MPa
PR	0.32	0.34
CTE	42 ppm/°C	102 ppm/°C

Figure 4. The specimens and specific printing process of the multifunctional mechanical metamaterial.

printing process, PVA/PA materials are alternately deposited to achieve a specific distribution of the heterogeneous materials. The out-of-plane thickness of all printed samples is 1 mm. By optimizing the process parameters (Table S1 of Supplementary Material), ensure that the manufacturing tolerance of the prepared samples is within ±0.13 mm. The equivalent performance of the fabricated structure was tested through temperature and mechanical loading: 1) The specimen was placed on a heated platform and uniformly heated from 20°C to 50°C; 2) The specimen was subjected to uniaxial tensile testing using a universal testing machine. During the loading process, macroscopic deformation of the specimen was recorded using a Nikon digital camera. Finally, the boundary dimension changes of the specimen under different loads were measured using image processing software ImageJ to calculate the equivalent performance.

3. Analysis of effective performances

This section systematically analyzed the macroscopic effective performance characteristics of multifunctional mechanical metamaterial through theory and FEA. For the analysis, all length quantities are normalized against the rectangle length a, elastic moduli against the YM E_{PVA} of PVA, and CTE against that of PA α_{PA} of PA. In all examples in this section, the in-plane thicknesses of M1 and M2 are equal ($t_1 = t_2$), and the rotating-rectangle length a is 0.05 m. In this section, unless otherwise noted, M1 and M2 are PA and PVA, respectively.

3.1. Relative porosity

Considering the RVE as shown in Figure 2, under the idealized assumption of neglecting interface overlapping effects, the theoretical mass density (ρ_r) and porosity (n_r) of the multifunctional mechanical metamaterial can be derived from the volume fraction theory as:

$$\rho_r = \frac{2t_1\rho_1((a+b+2r)\cos\theta-2r\sin\theta) + 2t_2\rho_2\left(a+b+\sqrt{a^2+b^2}+2r\right)}{(2r\cos\theta+b\sin\theta+a\cos\theta)(2r\cos\theta+a\sin\theta+b\cos\theta)} \tag{7}$$

$$n_r = \frac{2t_1((a+b+2r)\cos\theta-2r\sin\theta) + 2t_2\left(a+b+\sqrt{a^2+b^2}+2r\right)}{(2r\cos\theta+b\sin\theta+a\cos\theta)(2r\cos\theta+a\sin\theta+b\cos\theta)} \tag{8}$$

where ρ_1 and ρ_2 represent the densities of M1 and M2, respectively. Analytical expressions of Equations (7) and (8) reveals that the relative mass density of the structure exhibits a linear dependence on the densities of its constituent materials (ρ_1, ρ_2), and that the porosity is exclusively determined by the geometric parameters ($a, b, r, \theta, t_1, t_2$), demonstrating independence from material properties.

Figure 5 illustrates the influence of geometric parameters on the relative porosity of multifunctional mechanical metamaterials. Comparative analysis of four characteristic configurations (Figure 5a) demonstrates that increasing rotating-rectangle width b, rotation angle θ, and lateral extension length r enhances the effective area of the RVE. Consequently, under constant in-plane thickness (t_1 and t_2) of M1 and M2, these dimensional expansions induce significant porosity reduction through RVE area amplification, as evidenced in Figure 5b. Conversely, the in-plane thickness (t_1 and t_2) of M1 and M2 modifications regulate porosity through an alternative mechanism: while maintaining constant RVE area, adjustments in t_1 or t_2 alter the volumetric distribution of constituent materials, resulting in a systematic porosity elevation with increasing thickness (Figure 5b). Through simultaneously adopting rotating-rectangle width b, rotation angle θ and lateral extension length r to their geometric limits (here $t_1/a = t_2/a = 0.04$), extreme parameter combinations yield the maximum (0.34) and minimum (0.20) relative porosity values (Figure 5c). Furthermore, since rotation angle θ and lateral extension length r change the RVE's geometric size in both x and y directions, while rotating-rectangle width b only affects the y direction size, the first two parameters are much better than the latter in regulating the relative porosity.

3.2. Effective young's modulus

The effective YM is derived in Appendix (A.14) and (A.20) of Supplementary Material. We find that

a

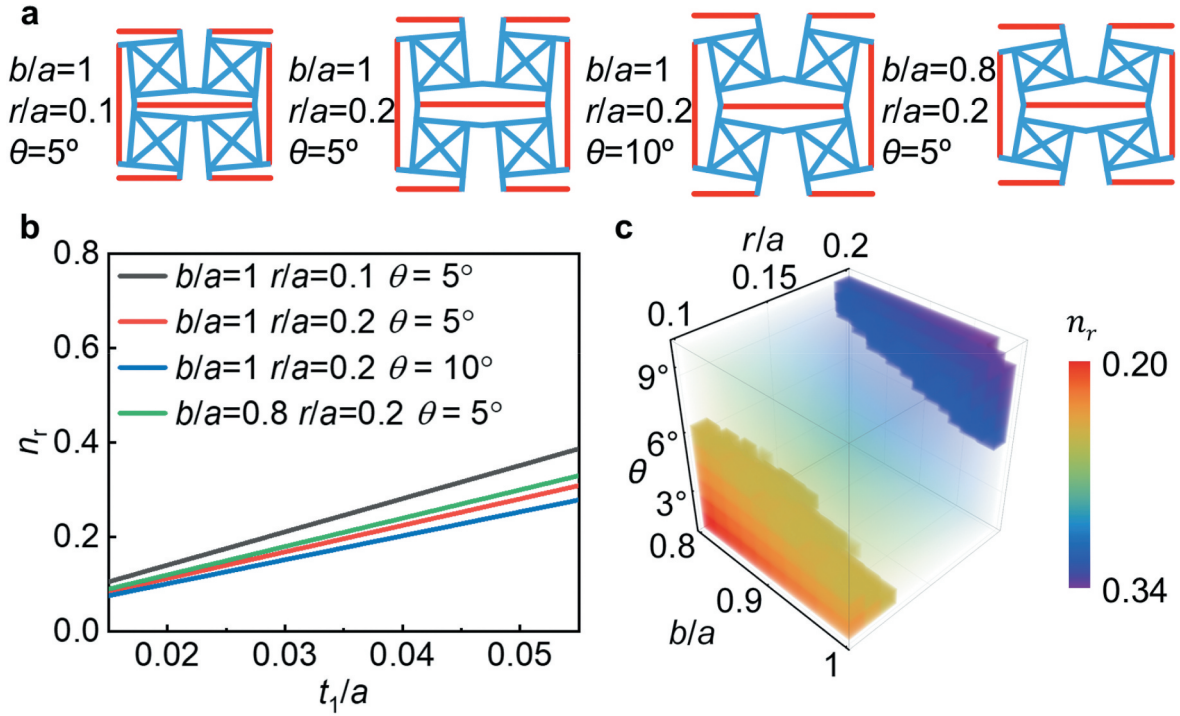**b**   **c**

Figure 5. The influence of geometric parameters on relative porosity: (a) four typical structures with different geometric parameters, (b) the relationship between t_1/a and relative porosity, (c) the relationship between b/a, θ and r/a and relative porosity.

$$\begin{cases} \bar{E}_{xx} = \dfrac{\bar{\sigma}_{xx}}{\bar{\varepsilon}_{xx}} = \dfrac{LE_2}{2Wc_3} \\ \bar{E}_{yy} = \dfrac{\bar{\sigma}_{yy}}{\bar{\varepsilon}_{yy}} = \dfrac{WE_2}{2Lc_2} \end{cases} \quad (9)$$

Here c_2 and c_3 are functions of geometric parameters (a, b, θ, t_1, t_2) and material parameters (E_1, E_2, E_2), given in Equation (B.73) of Appendix B of Supplementary Material. **L** and W represents the length and width of the quarter RVE, expressed as $2r\cos\theta + a\sin\theta + b\cos\theta$ and $2r\cos\theta + b\sin\theta + a\cos\theta$.

The influence of geometric parameters on the effective YM of multifunctional mechanical metamaterials is shown in Figure 6. The stress distribution of the RVE under tensile loading in x or y directions (Figure 6a) indicates that the maximum stress always occurs at the lateral extension of the rotating rectangle (here $b/a = 0.8$, $r/a = 0.2$, $\theta = 5°$ and $t_1/a = t_2/a = 0.04$). This is due to the fact that, during the stretching process, the lateral extension is simultaneously subjected to the coupled deformations of tension/compression, bending, and shear of the three beams connected at the rotating rectangle. The in-plane thickness (t_1 and t_2) of M1 and M2 shows a positive correlation with the effective YM ($\bar{E}_{xx}$ and $\bar{E}_{yy}$) in both the x and y directions (Figure 6b,c). When the aspect ratio (b/a) of the rotating rectangle is 1, the effective YM exhibits orthotropic isotropy, i.e. $\bar{E}_{xx} = \bar{E}_{yy}$; When the aspect ratio (b/a) of the rotating rectangle is less than 1, it changes to orthogonal anisotropy and the effective YM $\bar{E}_{yy}$ in the y direction is less than that $\bar{E}_{xx}$ in the x direction. Additionally, it can be observed that the YM in both directions decrease as lateral extension length r increases and increase as rotation angle θ increases (Figure 6d,e); rotating-rectangle width b exhibits an inverse regulation characteristic – its decrease causes the modulus in the x-direction to increase while the modulus in the y direction decreases. It is worth noting that, compared to lateral extension length r and rotating-rectangle width b, the modulus in both directions is significantly more sensitive to changes in rotation angle θ, indicating that rotation angle θ plays a dominant role in modulus regulation.

3.3. Effective poisson's ratio

The effective PR is derived in Appendix (A.15) and (A.21) of Supplementary Material. We find that
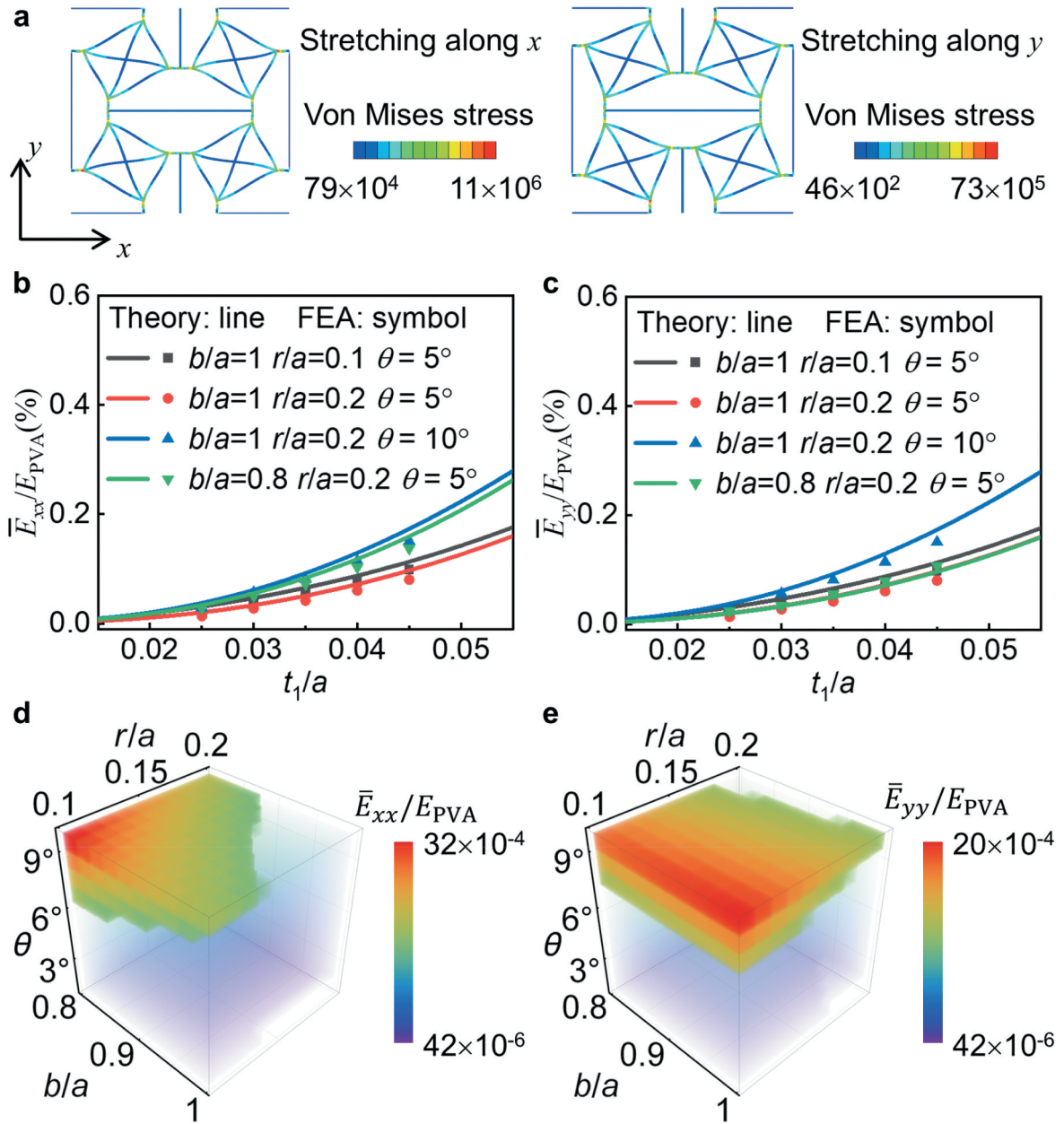
Figure 6. The influence of geometric parameters on effective YM: (a) the stress distribution of the RVE under tensile loading in x or y directions, (b) the relationship between t_1/a and $\bar{E}_{xx}$, (c) the relationship between t_1/a and $\bar{E}_{yy}$, (d) the relationship between $b/a,\theta$ and r/a and $\bar{E}_{xx}$, (e) the relationship between b/a, θ and r/a and $\bar{E}_{yy}$.

$$\begin{cases} \bar{v}_{yx} = -\dfrac{\bar{\varepsilon}_{xx}}{\bar{\varepsilon}_{yy}} = -\dfrac{Wc_3}{Lc_2} \\ \bar{v}_{xy} = -\dfrac{\bar{\varepsilon}_{yy}}{\bar{\varepsilon}_{xx}} = -\dfrac{Lc_3}{Wc_2} \end{cases} \tag{10}$$

Figure 7 shown the influence of geometric parameters on the effective PR of multifunctional mechanical metamaterials. By comparing the morphological evolution before and after stretching (Figure 7a), it is evident that the RVE exhibits a lateral expansion behavior when stretched in the x/y directions, showing an auxetic character (here $b/a = 0.8$, $r/a = 0.2$, $\theta = 5°$ and $t_1/a = t_2/a = 0.04$). When the aspect ratio (b/a) of the rotating rectangle is less than 1, the effective PR exhibits orthotropic anisotropic behavior: the absolute value of the effective PR $\bar{v}_{yx}$ along the x direction is significantly greater than the absolute value of $\bar{v}_{xy}$ along the y direction (Figure 7b,c). Linear increments in the in-plane thickness (t_1 and t_2) of M1 and M2 induce proportional reductions in PR
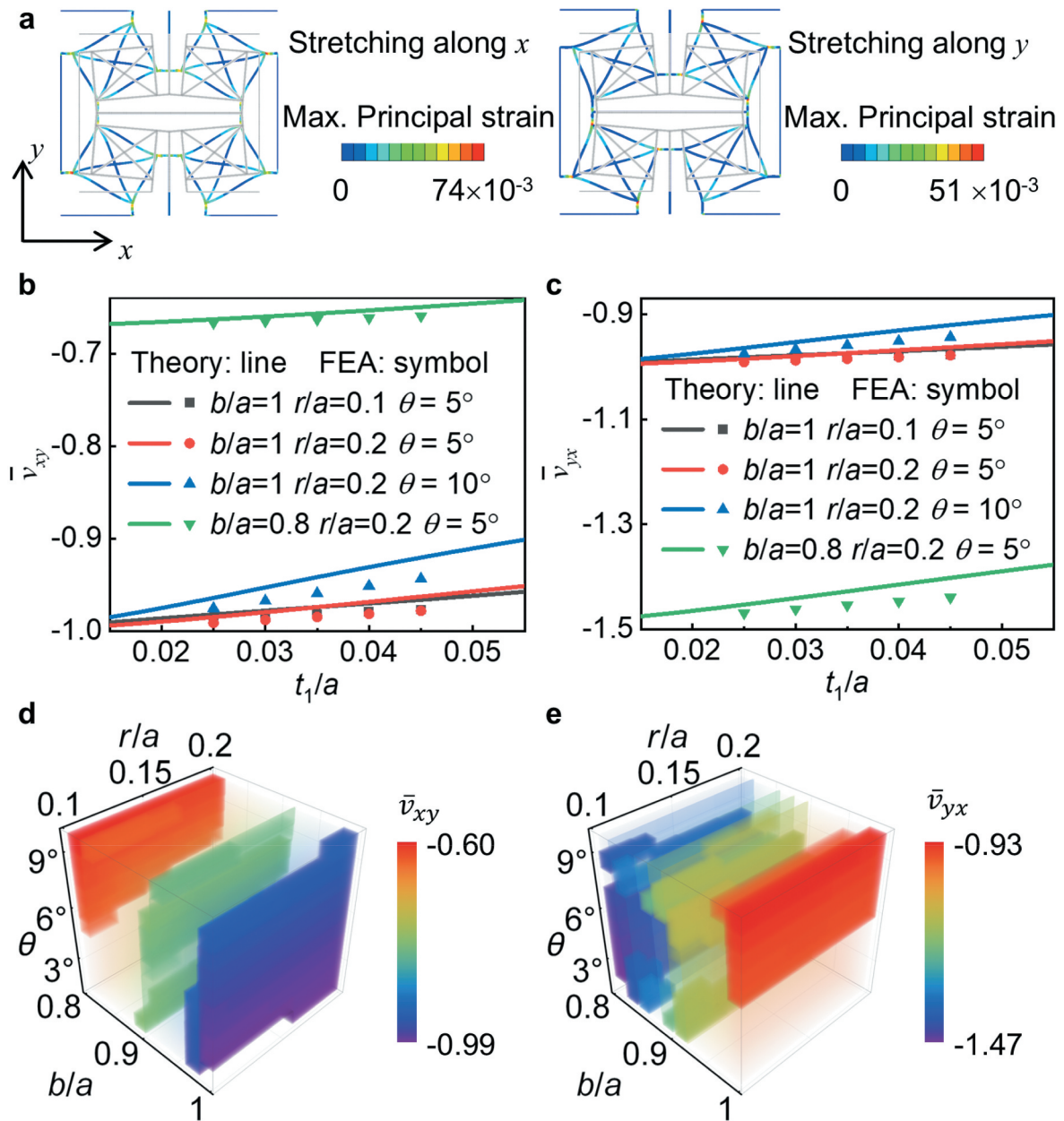
Figure 7. The influence of geometric parameters on effective PR: (a) the deformation shape of the RVE under tensile loading in x or y directions, (b) the relationship between t_1/a and $\bar{v}_{xy}$, (c) the relationship between t_1/a and $\bar{v}_{yx}$, (d) the relationship between b/a, θ and r/a and $\bar{v}_{xy}$, (e) the relationship between b/a, θ and r/a and $\bar{v}_{yx}$.

magnitudes for both directions. Within the given parameter range ($b/a = 0.8 - 1$, $\theta = 1° - 10°$ and $r/a = 0.1 - 0.2$), the effective PR consistently maintains negative values (Figure 7d,e). Lateral extension length r and rotating-rectangle width b have a symmetric effect on effective PR: a decrease in either of them reduces $\bar{v}_{xy}$ while increasing $\bar{v}_{yx}$. Conversely, reducing rotation angle θ simultaneously enhances both directional the absolute values of effective PR. Comparatively, the effective PR exhibits heightened sensitivity to rotating-rectangle width b variations relative to other two geometric parameters (r and θ).

3.4. Effective thermal expansion coefficient

The effective PR is derived in Appendix (A.27) of Supplementary Material. We find that

$$\begin{cases} \bar{a}_{xx} = \frac{\bar{\varepsilon}_{xx}}{\Delta T} = \frac{2g_3}{L} \\ \bar{a}_{yy} = \frac{\bar{\varepsilon}_{yy}}{\Delta T} = \frac{2g_2}{W} \end{cases} \tag{11}$$

Here g_2 and g_3 are expressed through geometric parameters ($a, b, r, \theta, t_1, t_2$) and material parameters (E_1, E_2, v_2, a_1, a_2), as provided in Equations (B.84) of Appendix B of Supplementary Material.

According to Equation (A.27), the effective CTE of multifunctional mechanical metamaterials is dependent not only on the microstructural geometry but also on the thermal expansion properties of its constituent materials. If the constituent materials have the same CTE, the effective CTE will be identical to that of the constituent materials, regardless of the microstructural configuration. Therefore, to achieve tunability of the CTE, it is necessary to employ two materials with different CTEs, applying them separately to the non-inclined and inclined beams, respectively. This leverages the thermal strain mismatch at the interface of the dissimilar materials to change macroscopic thermal deformation of structures.

To realize tunable macroscopic thermal contraction or expansion, two material combinations are considered: M1 and M2 are PA and PVA, respectively (Figure 8); and M1 and M2 are PVA and PA, respectively (Figure 9). Figure 8 illustrates the influence of geometric parameters on the effective CTE of multifunctional mechanical metamaterial when M1 is PA and M2 is PVA ($a_1 = a_{PA} > a_2 = a_{PVA}$). Under these conditions, the RVE exhibits macroscopic thermal contraction upon heating (Figure 8a, here $b/a = 0.8, r/a = 0.2$, $\theta = 5°$ and $t_1/a = t_2/a = 0.04$) Similarly, when the aspect ratio b/a of the rotating rectangle is less than 1, the effective CTE exhibits orthotropic anisotropy, with the absolute value of the CTE $\bar{a}_{xx}$ along the x direction being smaller than that $\bar{a}_{yy}$ along the y direction (Figure 8b,c). The absolute values of the CTEs in both directions decrease linearly with increasing the in-plane thickness (t_1 and t_2) of M1 and M2. Consistent with the trend observed for the effective PR, the effective CTEs in both directions remain negative (Figure 8d,e) within the given parameter range ($b/a = 0.8 - 1$, $\theta = 1° - 10°$ and $r/a = 0.1 - 0.2$). Lateral extension length r and rotation angle θ have the same effect on the effective CTEs in both directions; a decrease in either of them leads to an increase in the absolute values of the CTEs in both directions. A decrease in rotating-rectangle width b reduces the CTE $\bar{a}_{xx}$ along the x direction while increasing the CTE $\bar{a}_{yy}$ along the x direction. The variation of rotation angle θ has a more significant influence on the effective CTEs in both directions, whereas the influences of other two parameters (b and r) are relatively smaller.

Figure 9 shows the influence of geometric parameters on the effective CTE of multifunctional mechanical metamaterial after interchanging the positions of PA and PVA ($a_1 = a_{PVA} < a_2 = a_{PA}$). The results indicate that, in this case, the RVE exhibits macroscopic thermal expansion upon heating (Figure 9a), and all effective CTEs are positive (Figure 9b–e). The influence of the geometric parameters on the effective CTE remains consistent with the case where M1 and M2 are PA and PVA, respectively.

3.5. Synergistic adjustment

The above analysis indicates that the density, YM, PR, and CTE of the multifunctional mechanical metamaterial are synergistically influenced by its geometric parameters. When material parameters and other geometric parameters are fixed, increasing the relative in-plane thickness (t_1/a and t_2/a) enhances density and YM, whereas it reduces the absolute values of PR and CTE. When material parameters and in-plane thickness are fixed, decreasing the aspect ratio b/a increases density and the absolute value of CTE ($\bar{a}_{yy}$) while decreasing the absolute value of YM (E_{yy}) and the absolute value of PR ($\bar{v}_{yx}$); similarly, decreasing the rotation angle θ increases density and the absolute value of CTE while decreasing the absolute value of YM and the absolute value of PR ($\bar{v}_{yx}$); and decreasing the relative lateral extension length r/a increases density, YM, and the absolute value of CTE while decreasing the absolute value of PR ($\bar{v}_{yx}$). In summary, the synergistic adjustment of the various properties of this multifunctional mechanical metamaterial affects each other, necessitating trade-offs among its properties during design and fabrication.
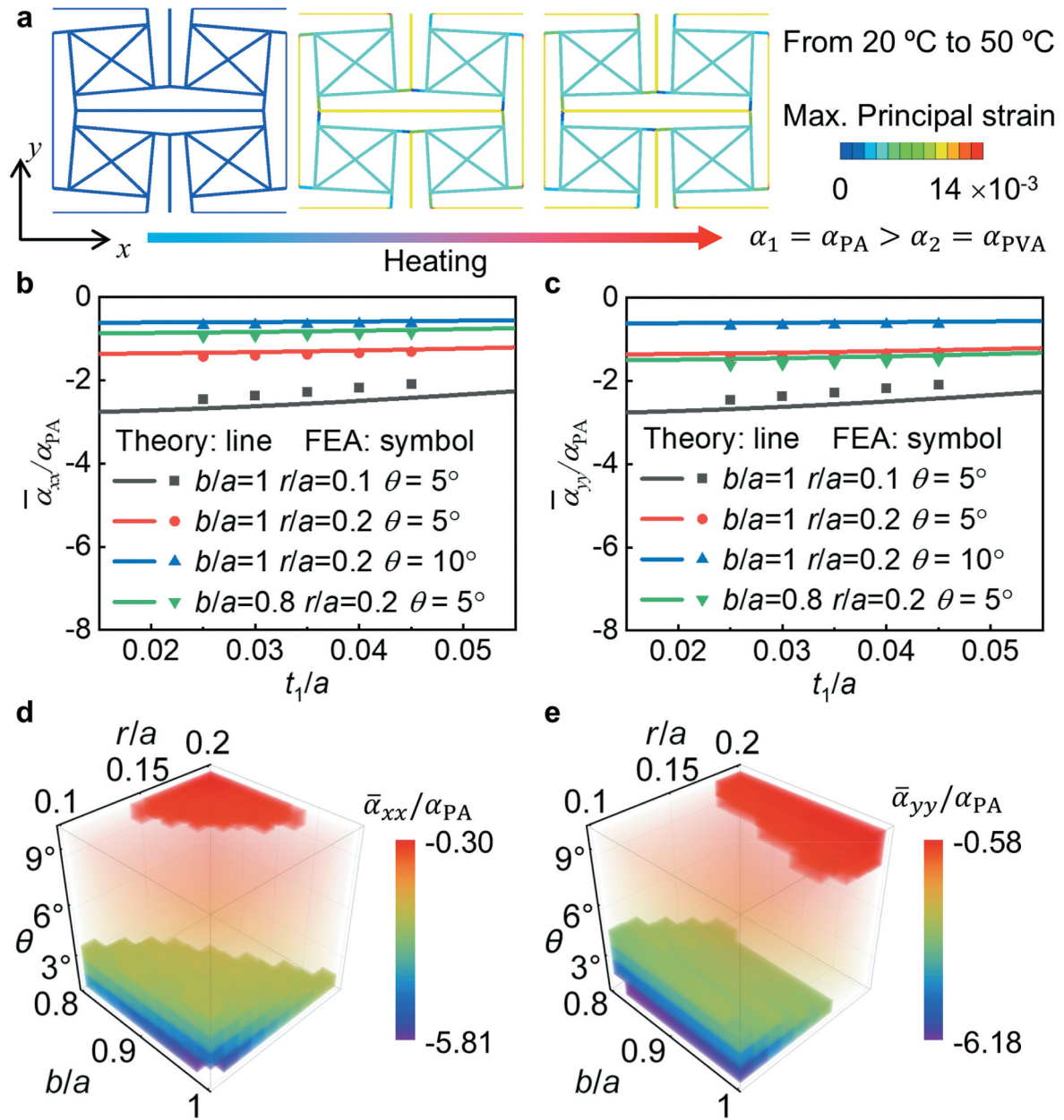
Figure 8. The influence of geometric parameters on effective CTE when material 1 is PA and material 2 is PVA: (a) the deformation shape of the RVE under temperature loading, (b) the relationship between t_1/a and $\bar{\alpha}_{xx}$, (c) the relationship between t_1/a and $\bar{\alpha}_{yy}$, (d) the relationship between b/a, θ and r/a and $\bar{\alpha}_{xx}$, (e) the relationship between b/a, θ and r/a and $\bar{\alpha}_{yy}$.

4. Experimental verification

4.1. Elastic constant test

A representative metamaterial was fabricated using fused deposition modeling 3D printing technology, and its PR and YM were tested and compared with theoretical and FEA results, as shown in Figure 10. The M1 and M2 of the representative metamaterial are PA and PVA, respectively. Its geometric parameters were shown in Figure 10a. From Figure 10a, it is evident that the specimen exhibits a distinct outward expansion in the orthogonal direction during uniaxial tension. The measured PR from the experiment (Exp.) is approximately −1.36, which closely matches the theoretical and FEA values (1.47). During the uniaxial tensile test, the stress-strain curve of the specimen demonstrates a linear variation from strain 0 to 17%, indicating good structural
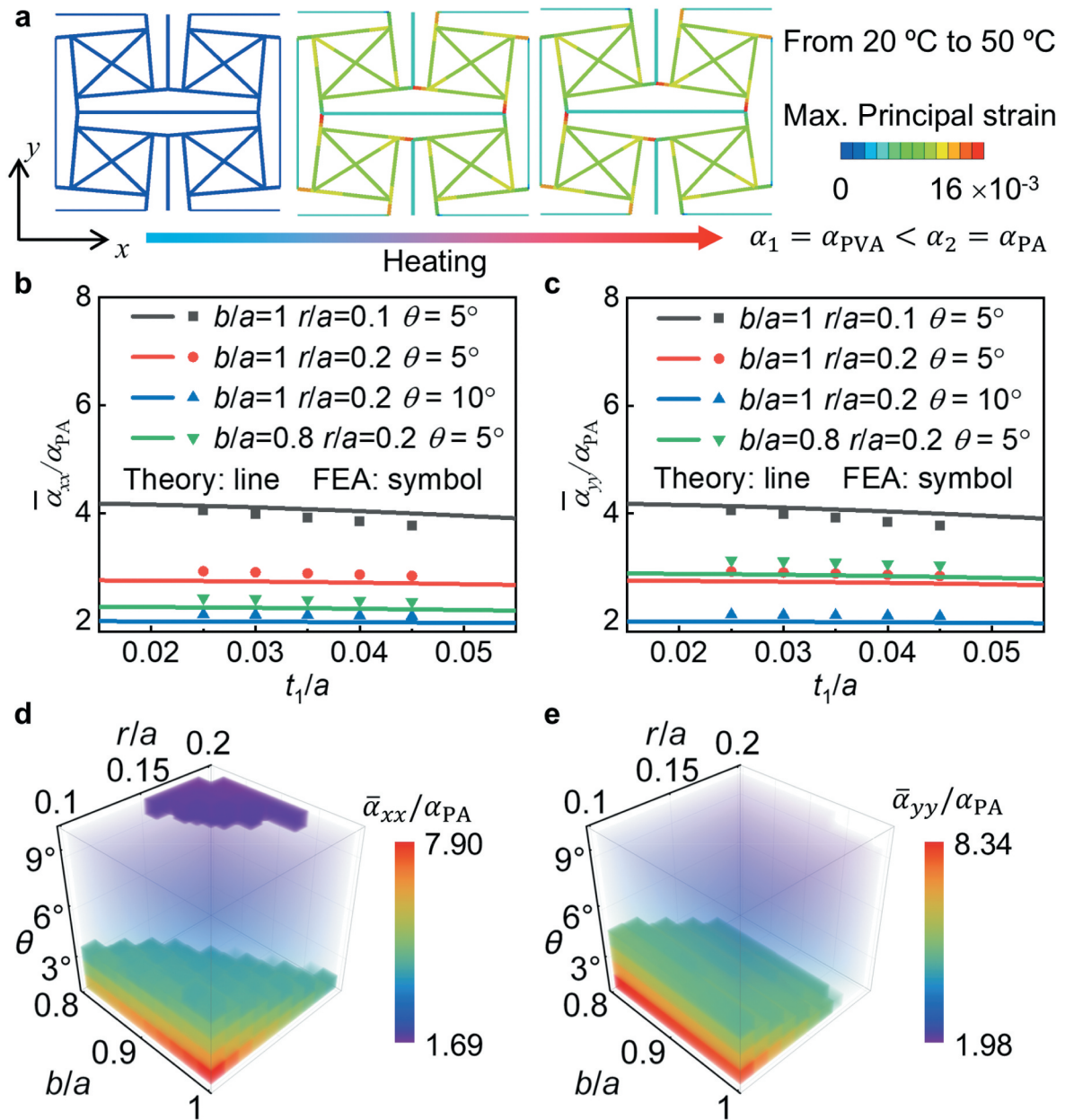
Figure 9. The influence of geometric parameters on effective CTE when material 1 is PVA and material 2 is PA: (a) the deformation shape of the RVE under temperature loading, (b) the relationship between t_1/a and $\bar{\alpha}_{xx}$, (c) the relationship between t_1/a and $\bar{\alpha}_{yy}$, (d) the relationship between b/a, θ and r/a and $\bar{\alpha}_{xx}$, (e) the relationship between b/a, θ and r/a and $\bar{\alpha}_{yy}$.

stability. The measured YM from the Exp. is approximately 0.831 MPa, slightly higher than the theoretical and FEA results, with a maximum relative deviation of about 20%. This deviation is primarily attributed to the combined effects of inevitable manufacturing tolerances in the complex geometry, which can lead to subtle positive deviations in key dimensions like beam thickness and rotation angle, and potential differences between the effective material properties within the printed specimen and the nominal values obtained from bulk coupon tests. Furthermore, simplifications in the analytical model and boundary conditions in the FEA versus experiments may also contribute.
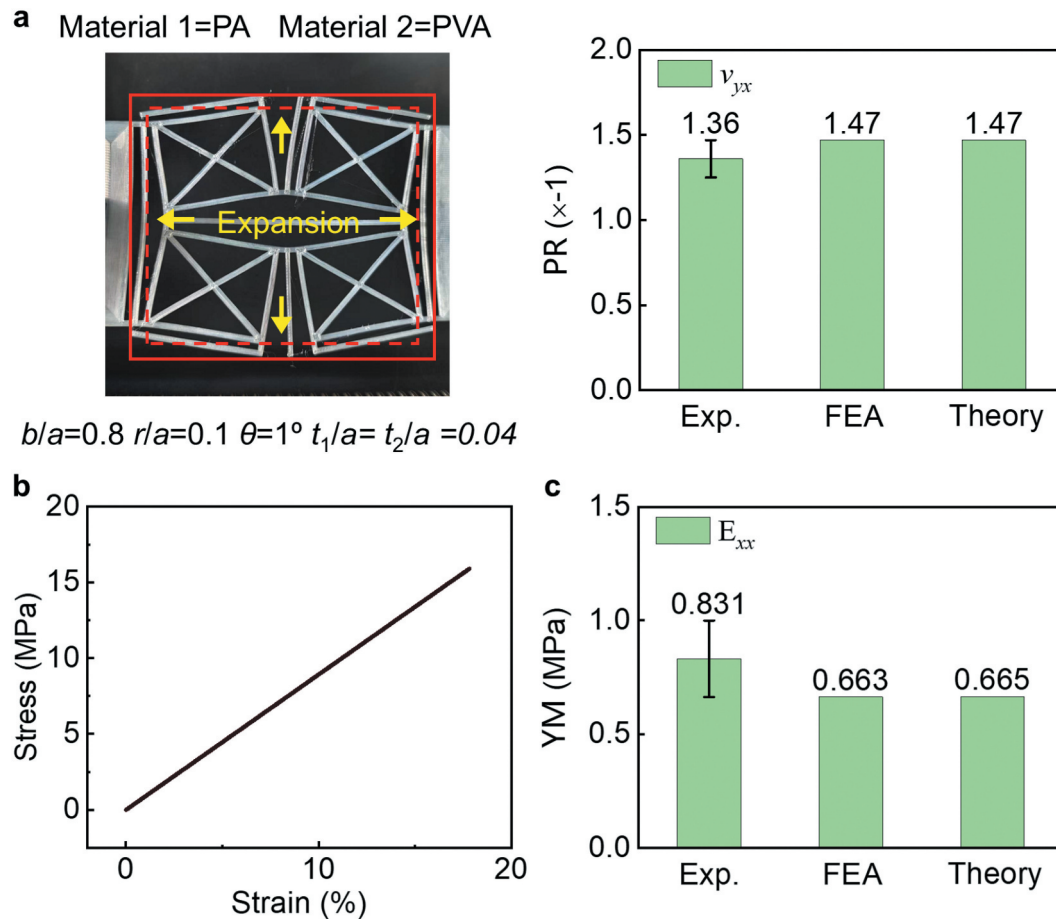
Figure 10. Elastic constant test: (a) the specimen under tension, (b) PR of Exp., FEA and theory, (c) the stress-strain curve of the specimen, (d) YM of Exp., FEA and theory.

4.2. Thermal expansion coefficient test

In the CTE tests, two types of metamaterials with different material distributions were fabricated, as shown in Figure 11. Figure 11a shows that when M1 and M2 are PA and PVA respectively, the specimen exhibits significant thermal shrinkage deformation in orthogonal directions during heating. The experimentally measured CTEs in orthogonal directions for this specimen are approximately −354 and −564 ppm/°C (Figure 11a), with a maximum deviation of 12% from theoretical and FEA results. When the positions of the two materials are exchanged while keeping geometric parameters unchanged (i.e. M1 and M2 are PVA and PA respectively), the specimen exhibits significant thermal expansion deformation in orthogonal directions during heating (Figure 11b). The experimentally measured CTEs in orthogonal directions for this specimen are approximately 539 and 755 ppm/°C (Figure 11b), with a maximum deviation of 11% from theoretical and FEA results. These results demonstrate that the proposed metamaterials can be successfully manufactured using fused deposition modeling 3D printing technology, and the experimentally obtained properties show good agreement with theoretical and FEA predictions. Furthermore, it can be foreseen that the stress concentrations at material interfaces are typically higher than in other regions, making interfaces vulnerable to delamination failure for the multifunctional mechanical metamaterials composed of heterogeneous materials.

5. Comparison with other materials

To illustrate the unique properties achievable, Figure 12 presents a performance comparison between two multifunctional mechanical metamaterials and natural and artificial materials, and metamaterials reported in existing literature. Two multifunctional mechanical metamaterials (Figure 12a) possess identical geometric
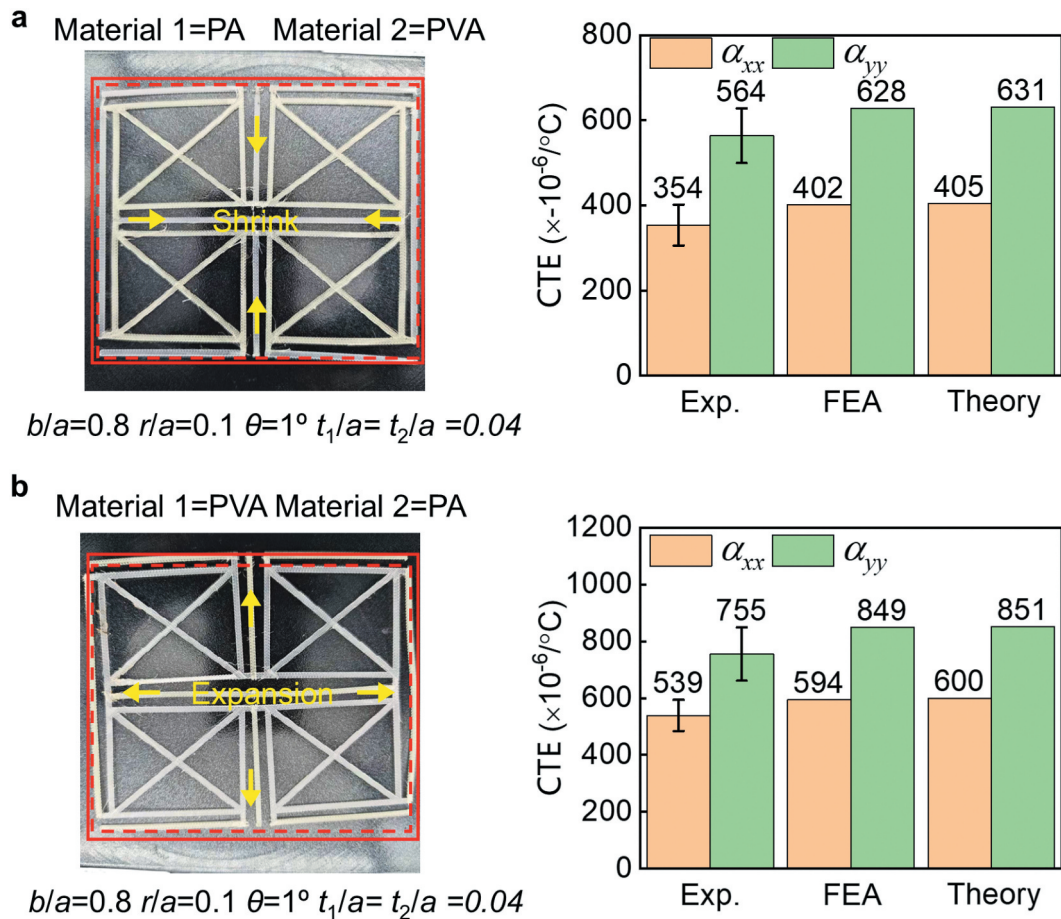
Figure 11. Thermal expansion coefficient test: (a) the specimen under heating and CTE of Exp., FEA and theory when M1//M2 is PA/PVA, (c) the specimen under heating and CTE of Exp., FEA and theory when M1//M2 is PVA/PA.
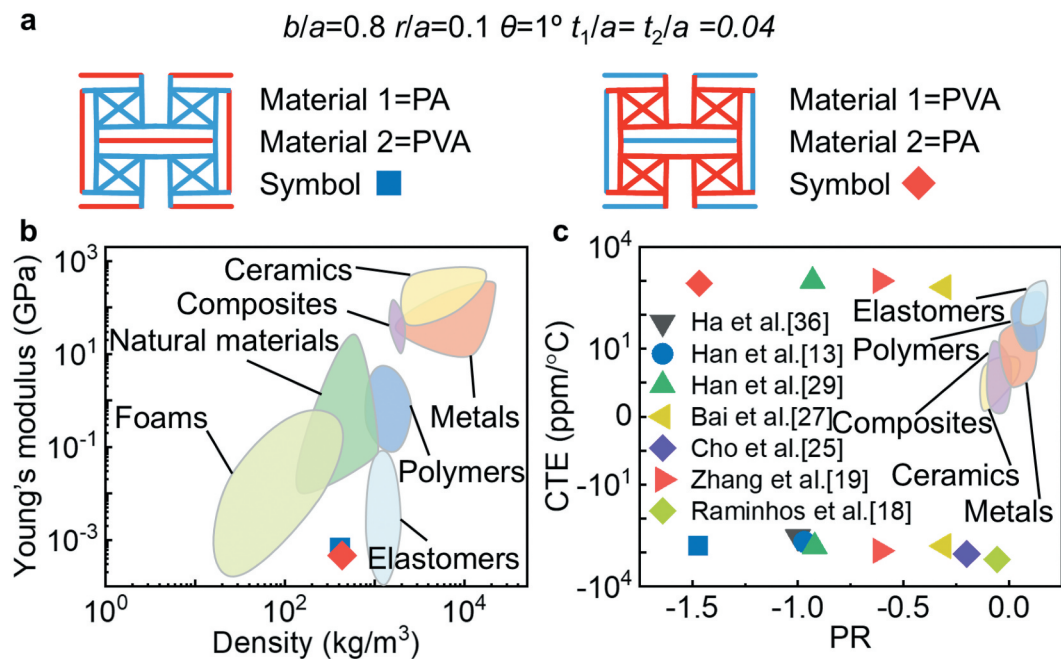

Figure 12. Comparison with other materials: (a) two metamaterials with the same geometric parameters but different material distributions, (b) comparison of YM and density, (c) comparison of CTE and PR [13,18,19,25,27,29,36].

parameters (here $b/a = 0.8, r/a = 0.1, \theta = 1°$ and $t_1/a = t_2/a = 0.04$) but distinct material distributions (blue symbol: M1/M2 = PA/PVA; red symbol: M1/M2 = PVA/PA). Compared to conventional material systems, the structures designed in this study exhibit the following characteristics: (1) low densities (blue symbol: 0.42 g/cm^3; red symbol: 0.44 g/cm^3) on the order of magnitude of natural materials and low YM $\bar{E}_{yy}$(blue symbol: 67 MPa; red symbol: 46 MPa) on the order of magnitude of foams (Figure 12c); (2) simultaneous negative PR $\bar{v}_{yx}$ (blue symbol: −1.47; red symbol: −1.47) and amplified, positive (blue symbol: −630 ppm/°C) or negative (red symbol: 850 ppm/°C) CTE $\bar{\alpha}_{yy}$ (Figure 12d). The coupled realization of negative PR and negative CTE is typically difficult to achieve in natural materials (with a few exceptions such as zeolites) and existing artificial materials. However, the proposed configuration, through synergistic geometric design and material distribution, overcomes this limitation. Furthermore, PR in this study is higher than that reported in existing literature (Figure 12d), while CTE is almost the same.

6. Conclusions

In summary, this paper reports a multifunctional mechanical metamaterial that achieves tunable density, stiffness, Poisson's ratio, and thermal expansion coefficient through careful geometric design and material distribution. A combination of theoretical analysis and finite element simulations was used to systematically investigate the influence of various geometric parameters on the effective properties of the metamaterial. The study found that adjusting the dimensions of the rotating rectangles, the rotation angle, the in-plane thickness of the constituent materials and lateral extension length allows for effective control over the relative porosity, effective Young's modulus, Poisson's ratio, and thermal expansion coefficient. Notably, by modifying the material distribution, the metamaterial can exhibit either macroscopic thermal contraction or thermal expansion upon heating. Compared to conventional material systems, the designed metamaterial integrates low density, high adaptability, negative Poisson's ratio, and a tunable (positive or negative) thermal expansion coefficient. This combination of properties is rarely achieved in natural or existing artificial materials. Furthermore, the theoretical and numerical results showed good agreement, validating the accuracy of the theoretical model. This work not only provides a theoretical foundation for the design and optimization of multifunctional mechanical metamaterials but also offers new avenues for their application in smart structures and thermal management.

Disclosure statement

Funding

References

[1] T. Liu, C. Lin, Y. Zhang, J. Cai, and J. Yang, *Viscoelastic negative stiffness metamaterial with multistage load bearing and programmable energy absorption ability*, Int. J. Smart Nano Mater. 16 (2024), pp. 1–23. doi:10.1080/19475411.2024.2428172.

[2] T. Liu, W. Zhao, Y. Yao, C. Lin, H. Zhao, and J. Cai, *Mechanical and shape-memory properties of TPMS with hybrid configurations and materials*, Int. J. Smart Nano Mater. 15 (2024), pp. 786–810. doi:10.1080/19475411.2024.2410289.

[3] X. Yu, J. Zhou, H. Liang, Z. Jiang, and L. Wu, *Mechanical metamaterials associated with stiffness, rigidity and compressibility: A brief review*, Prog. Mater. Sci. 94 (2018), pp. 114–173. doi:10.1016/j.pmatsci.2017.12.003.

[4] C. Zeng, L. Liu, Y. Hu, W. Zhao, X. Xin, Y. Liu, and J. Leng, *Stair-Stepping mechanical metamaterials with programmable load plateaus*, Adv Funct Mater. 34 (2024), doi:10.1002/adfm.202408887.

[5] P. Xu, X. Lan, C. Zeng, X. Zhang, H. Zhao, J. Leng, and Y. Liu, *Compression behavior of 4D printed metamaterials with various poisson's ratios*, Int. J. Mech. Sci. 264 (2024), pp. 108819. doi:10.1016/j.ijmecsci.2023.108819.

[6] N.G.-C. James, A. Daphne, N.G. Joseph, and E.E. Kenneth, *Auxetic behavior and other negative thermomechanical properties from rotating rigid units*, Phys. Status Solidi 16 (2022), pp. 2100322. doi:10.1002/pssr.202100322.

[7] Y. Kim, K.H. Son, and J.W. Lee, *Auxetic structures for tissue engineering scaffolds and biomedical devices*, Mater (Basel) 14 (2021), pp. 6821. doi:10.3390/ma14226821.

[8] H. Xu, H.-T. Liu, and G.-F. Li, *In-plane characteristics of a multi-arc re-entrant auxetic honeycomb with enhanced negative poisson's ratio effect and energy absorption*, Eur. J. Mech. A. Solids 109 (2025), pp. 105473. doi:10.1016/j.euromechsol.2024.105473.

[9] W. Xu, X. Xiao, J. Chen, Z. Han, and K. Wei, *Program multi-directional thermal expansion in a series of bending dominated mechanical metamaterials*, Thin-Walled Struct. 174 (2022), pp. 109147. doi:10.1016/j.tws.2022.109147.

[10] Z. Xu, H. Zhao, and K. Wang, *Design of hourglass-lattice metastructure with near-zero thermal expansion using structural optimization method*, Eng. Struct. 277 (2023), pp. 115374. doi:10.1016/j.engstruct.2022.115374.

[11] J. Li, H.-T. Liu, and Z.-Y. Zhang, *Stiffness characteristics for bi-directional tunable thermal expansion metamaterial based on bi-material triangular unit*, Int. J. Mech. Sci. 241 (2023), pp. 107983. doi:10.1016/j.ijmecsci.2022.107983.

[12] L. Wu, B. Li, and J. Zhou, *Isotropic negative thermal expansion metamaterials*, ACS Appl. Mater. Interfaces 8 (2016), pp. 17721–17727. doi:10.1021/acsami.6b05717.

[13] Z. Han, X. Xiao, J. Chen, K. Wei, Z. Wang, X. Yang, and D. Fang, *Bifunctional metamaterials incorporating unusual geminations of poisson's ratio and coefficient of thermal expansion*, ACS Appl. Mater. Interfaces 14 (2022), pp. 50068–50078. doi:10.1021/acsami.2c11702.

[14] X.-L. Peng and S. Bargmann, *A novel hybrid-honeycomb structure: Enhanced stiffness, tunable auxeticity and negative thermal expansion*, Int. J. Mech. Sci 190 (2021), pp. 106021. doi:10.1016/j.ijmecsci.2020.106021.

[15] T.-C. Lim, *A metamaterial with negative thermal expansivity and programmable poisson's ratio based on rotating triangles and quivering rhombi*, Eur. J. Mech. A. Solids 100 (2023), pp. 104986. doi:10.1016/j.euromechsol.2023.104986.

[16] Y. Peng, K. Wei, M. Mei, X. Yang, and D. Fang, *Simultaneously program thermal expansion and poisson's ratio in three dimensional mechanical metamaterial*, Compos. Struct. 262 (2021), pp. 113365. doi:10.1016/j.compstruct.2020.113365.

[17] H. Yang and L. Ma, *1D to 3D multi-stable architected materials with zero poisson's ratio and controllable thermal expansion*, Mater. Des. 188 (2020), pp. 108430. doi:10.1016/j.matdes.2019.108430.

[18] J.S. Raminhos, J.P. Borges, and A. Velhinho, *Development of polymeric anepectic meshes: Auxetic metamaterials with negative thermal expansion*, Smart Mater. Struct. 28 (2019), pp. 045010. doi:10.1088/1361-665X/ab034b.

[19] X. Zhang, W. Zhu, R. Tian, L. Chen, and H. Guan, *Dual arrowhead-shaped re-entrant auxetic hybrid metamaterial with adjustable thermal expansion*, Mater. Today Commun. 40 (2024), pp. 109456. doi:10.1016/j.mtcomm.2024.109456 .

[20] W. Ye, Z. Zhou, and Q. Li, *Modelling and verification of a novel bi-material mechanical metamaterial cellular structure with tunable coefficient of thermal expansion*, Mater. Today Commun. 33 (2022), pp. 104940. doi:10.1016/j.mtcomm.2022.104940.

[21] L. Shen, K. Wei, K. Yuan, C. Shi, Z. Li, and Z. Wang, *A novel metamaterial incorporating both auxeticity and thermal shrinkage*, Int. J. Mech. Sci 233 (2022), pp. 233. doi:10.1016/j.ijmecsci.2022.107650.

[22] F. Lu, X. Chen, Y. Zhu, C. Zhang, and Y. Hou, *A novel re-entrant-type metamaterial with tunable negative poisson's ratios and coefficients of thermal expansion*, Int. J. Appl. Mech. 14 (2022), doi:10.1142/S1758825122500405.

[23] H.-T. Liu, N. Xu, Y.-B. Wang, and L. Wang, *Three-dimensional enhanced star-shaped honeycombs with negative thermal expansion*, Compos. Struct. 279 (2022), pp. 114772. doi:10.1016/j.compstruct.2021.114772.

[24] K.-J. Liu, H.-T. Liu, and J. Li, *Thermal expansion and bandgap properties of bi-material triangle re-entrant honeycomb with adjustable poisson's ratio*, Int. J. Mech. Sci. 242 (2023), pp. 108015. doi:10.1016/j.ijmecsci.2022.108015.

[25] M.W. Cho, K. Ko, M. Mohammadhosseinzadeh, J.H. Kim, D.Y. Park, D.S. Shin, and S.M. Park, *Inverse design of bezier curve-based mechanical metamaterials with programmable negative thermal expansion and negative poisson's ratio via a data augmented deep autoencoder*, Mater Horiz. 11 (2024), pp. 2615–2627. doi:10.1039/D4MH00302K.

[26] T.-C. Lim, *Metamaterial with sign-toggling thermal expansivity inspired by Islamic motifs in Spain*, J. Sci.: Adv. Mater. Devices 7 (2022), pp. 100401. doi:10.1016/j.jsamd.2021.11.003.

[27] Y. Bai, C. Liu, Y. Li, J. Li, L. Qiao, J. Zhou, and Y. Bai, *Programmable mechanical metamaterials with tailorable negative poisson's ratio and arbitrary thermal expansion in multiple thermal deformation modes*, ACS Appl. Mater. Interfaces 14 (2022), pp. 35905–35916. doi:10.1021/acsami.2c08270.

[28] Z. Li, W. Gao, M. Yu Wang, and Z. Luo, *Design of multi-material isotropic auxetic microlattices with zero thermal expansion*, Mater. Des. 222 (2022), pp. 111051. doi:10.1016/j.matdes.2022.111051.

[29] Z. Han and K. Wei, *Multi-material topology optimization and additive manufacturing for metamaterials incorporating double negative indexes of poisson's ratio and thermal expansion*, Addit. Manuf. 54 (2022), pp. 102742. doi:10.1016/j.addma.2022.102742.

[30] K. Wang, J. Chen, Z. Han, K. Wei, X. Yang, Z. Wang, and D. Fang, *Synergistically program thermal expansional and mechanical performances in 3D metamaterials: Design-architecture-performance*, J. Mech. Phys. Solids 169 (2022), pp. 105064. doi:10.1016/j.jmps.2022.105064.

[31] H. Yu, H. Wang, B. Liang, and X. Guo, *Metamaterials with remarkable thermal–mechanical stability and high specific modulus: Mechanical designs, theoretical predictions and experimental demonstrations*, Extrem. Mech. Lett. 49 (2021), pp. 101436. doi:10.1016/j.eml.2021.101436.

[32] H. Xu, A. Farag, and D. Pasini, *Routes to program thermal expansion in three-dimensional lattice metamaterials built from tetrahedral building blocks*, J. Mech. Phys. Solids 117 (2018), pp. 54–87. doi:10.1016/j.jmps.2018.04.012.

[33] X.-L. Peng and S. Bargmann, *Tunable auxeticity and isotropic negative thermal expansion in three-dimensional lattice structures of cubic symmetry*, Extrem Mech. Lett. 43 (2021), pp. 101201. doi:10.1016/j.eml.2021.101201.

[34] J. Huang, W. Li, M. Chen, and M. Fu, *An auxetic material with negative coefficient of thermal expansion and high stiffness*, Appl. Compos Mater. 29 (2021), pp. 777–802. doi:10.1007/s10443-021-09983-y.

[35] J. Tian, J. Yang, and Y. Zhao, *Metamaterial with synergistically controllable poisson's ratio and thermal expansion coefficient*, Int. J. Mech. Sci. 256 (2023), pp. 108488. doi:10.1016/j.ijmecsci.2023.108488.

[36] C.S. Ha, E. Hestekin, J. Li, M.E. Plesha, and R.S. Lakes, *Controllable thermal expansion of large magnitude in chiral negative poisson's ratio lattices*, Phys. Status Solidi B 252 (2015), pp. 1431–1434. doi:10.1002/pssb.201552158.